α-Cyperone targets the PAK1-JNK/NF-κB axis to modulate dendritic cells maturation and Th2/Th9 differentiation in an asthma model

HANG HU[1*], XING WANG[2*], LINLIN GUO[3*], ZILING ZENG[4], HONGMEI TANG[2], YUN ZHANG[2], JIAYAO DUAN[2] and KAIJIN WANG[1]

[1]Department of Respiratory and Critical Care Medicine, Bishan Hospital of Chongqing, Bishan Hospital of Chongqing Medical University, Chongqing 402760, P.R. China; [2]Inflammation and Allergic Diseases Research Unit, The Affiliated Hospital of Southwest Medical University, Luzhou, Sichuan 646000, P.R. China; [3]Department of Microbiology and Immunology, Indiana University School of Medicine, Indianapolis, IN 46202, USA; [4]Department of Respiratory and Critical Care Medicine, Deyang People's Hospital, Deyang, Sichuan 618000, P.R. China

Received December 17, 2025; Accepted July 23, 2026

DOI: 10.3892/ijmm.2026.5957

Abstract. Asthma is a common chronic airway inflammatory disease affecting millions of patients worldwide, and its treatment remains a clinical challenge. A variety of immune cells, cytokines and inflammatory mediators are associated with asthmatic pathogenesis. The α-Cyperone (CYP) is the active ingredient of *Cyperus rotundus* L., which exhibits significant anti-inflammatory effects in numerous diseases. However, whether and how CYP plays a role in allergic asthma has not yet been reported. It was found that CYP inhibits airway inflammation and mucus hypersecretion in a mouse allergic asthma model by reducing the proportion of mature dendritic cells (DCs) and the differentiation of Th2 and Th9 cells in lung tissue and mediastinal lymph nodes. Furthermore, CYP inhibits DCs maturation via the PAK1-JNK/nuclear factor-κB (NF-κB) pathway, thereby attenuating subsequent Th2 and Th9 cell differentiation. Moreover, it was found that IL-33 can promote the differentiation of naïve T cells into Th2/Th9 by activating PAK1-JNK/NF-κB signaling. CYP decreases this IL-33-induced Th2/Th9 differentiation by inhibiting the PAK1-JNK/NF-κB axis. The computational analysis indicates that CYP binds to the PAK1 protein at Ser144 that verified by Biacore surface plasmon resonance analyzes and kinase activity testing. Taken together, the present study demonstrated that CYP improves allergic asthma by targeting PAK1 to inhibit the PAK1-JNK/NF-κB pathway.

Correspondence to: Professor Kaijin Wang, Department of Respiratory and Critical Care Medicine, Bishan Hospital of Chongqing, Bishan Hospital of Chongqing Medical University, 9 Shuangxing Avenue, Bishan, Chongqing 402760, P.R. China
E-mail: wangkaixin2006521@126.com

*Contributed equally

Abbreviations: Akt, AKT serine/threonine kinase; ANOVA, analysis of variance; BMDCs, bone marrow DCs; CD, Cluster of differentiation; Cdc42, Cell division control protein 42 homolog; c-Jun, c-Jun N-terminal kinase (JNK)-mediated activated protein-1; CYP, α-Cyperone; DCs, dendritic cells; ECL, enhanced chemiluminescence; Eos, eosinophils; FACS buffer, fluorescence-activated cell sorting buffer; FBS, fetal bovine serum; H&E staining, hematoxylin and eosin staining; IFN, interferon; IL, interleukin; ILC2, group 2 innate lymphoid cells; i.p., intraperitoneal; Jag-1, jagged canonical Notch ligand 1; LPS, lipopolysaccharide; Lys, lysine; MHC-II, major histocompatibility complex class II; MLN, mediastinal lymph node; Neu, neutrophils; NF-κB, nuclear factor-κB; OVA, ovalbumin; OT-II, OVA-specific T-cell receptor transgenic mice; PAK1, p21-activated kinase 1; p-PAK1, phosphorylated-PAK1; PAS, periodic acid-Schiff; PU.1/SPI1, spleen focus forming virus (SFFV) proviral integration oncogene 1; qPCR, quantitative polymerase chain reaction; Ser, serine; ST2, suppression of tumorigenicity 2; TB, Toluidine Blue; Th, T-helper; TGF, transforming growth factor; Thr, threonine; TNF, tumor necrosis factor

Key words: allergy, asthma, T cell; DCs, α-Cyperone, PAK1, JNK, NF-κB

Introduction

Asthma is a prevalent chronic airway inflammatory disease characterized by the involvement of various immune cells and inflammatory mediators. Despite affecting millions of individuals worldwide and it remains a significant global health challenge with limited efficacy. The α-Cyperone (CYP) is the primary bioactive compound derived from *Cyperus rotundus* L. that shows anti-inflammatory properties across various pathologies, including acute lung injury and neuroinflammation.

Dendritic cells (DCs) serve as pivotal mediators in the pathogenesis, progression and immune regulation of allergic asthma (1). Upon maturation, DCs facilitate the differentiation of naïve T cells (Th0) into various effector subsets cells by expressing high levels of co-stimulatory molecules such as

CD80, CD86 and CD40 (2). A central regulator of this process is nuclear factor-κB (NF-κB), a critical transcription factor in the human immune system that governs the development and regulation of DCs. Notably, inhibition of NF-κB has been shown to arrest the maturation of DCs (3). Evidence suggests CYP exerts potent anti-inflammatory effects by modulating these pathways. In lipopolysaccharide (LPS)-induced microglia, CYP activates the Akt/nuclear factor erythroid 2-related factor 2/heme oxygenase 1 axis while suppressing the NF-κB pathway, thereby reducing the inflammatory response (4). Furthermore, CYP has been shown to attenuate neuroinflammation through the STING signaling pathway (5) and protect against LPS-induced acute lung injury in murine models by upregulating SIRT1, which subsequently inhibits the NF-κB and nucleotide-binding oligomerization domain (NOD)-like receptors pyrin domain containing 3 signaling cascades (6). The functional landscape of DCs is further complicated by the interplay between NF-κB and c-Jun N-terminal kinase (JNK)-mediated activated protein-1 (c-Jun). These factors interact within DCs to co-regulate cellular function through multiple mechanisms such as negative feedback, transcriptional synergism, and the modulation of apoptosis (7). The related signaling components, such as p21-activated kinase 1 (PAK1), also play a role; for example, in the deficient of PAK1 leads to increased JNK expression and increased susceptibility to heart failure (8), while *Salmonella typhimurium* infection activates Cdc42 and PAK1 to trigger NF-κB inflammatory signaling (9). Despite these insights into the regulatory roles of CYP and its impact on related inflammatory pathways, its potential efficacy in alleviating allergic asthma remains to be elucidated.

IL-33 is a key mediator of allergic and chronic inflammatory pathologies (10). Research indicates that increased ST2 (the receptor for IL-33) expression on DCs promotes T helper 2 cell (Th2) polarization in allergic asthma (11), while interrupting IL-33/ST2 signaling prevents Dectin-1-induced the differentiation of Th9 cell (12). These findings suggest that targeting IL-33 could impede both Th2 and Th9 responses. While IL-33 is known to drive Th2 cell differentiation by activating the JNK-c-JUN/NF-κB signaling pathway through ST2 (13), and influence Th9 cell through PU.1 regulation (14). The specific role of the NF-κB and JNK-c-JUN signaling pathways in the Th9 development is also well documented (15,16). Nevertheless, it remains unclear if CYP can directly inhibit T cell differentiation into these specific subsets.

Evidence suggests CYP effectively attenuates lung inflammation in allergic asthma and may suppress DCs maturation by inhibiting PAK1 phosphorylation. Both *in vivo* and *in vitro* results indicate that CYP inhibit airway inflammation and mucus hypersecretion by reducing the proportions of mature DCs, Th2 and Th9 cells within lung tissue and mediastinal lymph node (MLN). This effect counteracts the IL-33-induced elevations of various immune cells mediated via the PAK1-JNK/NF-κB signaling. Consequently, the PAK1 signaling network represents a promising target, and CYP emerges as a potential candidate for the treatment of allergic asthma.

Materials and methods

Animal and experimental model. C57BL/6J 48 female mice (6-8 weeks old, weighing 18-22 g) were purchased from Gempharmatech Co., Ltd. Animals were housed under specific pathogen-free (SPF) conditions at the Animal Experimental Center of Southwest Medical University. The facility was maintained at a controlled temperature (22±2˚C) and humidity (50-60%) under a 12/12-h light/dark cycle, with *ad libitum* access to standard chow and water. To provide environmental enrichment, cages were supplied with paper balls and plastic tubes. All *in vivo* experimental procedures, including euthanasia, complied with the National Institutes of Health guidelines and were approved by the Institutional Animal Care and Use Committee of Southwest Medical University (approval nos. 20240417-002 and 20240701-007; Luzhou, China).

A murine model of allergic airway inflammation was induced using ovalbumin (OVA). Briefly, mice were sensitized via intraperitoneal (i.p.) injection with 20 μg of OVA (cat. no. HY-P0286; MedChemExpress) emulsified with 1 mg of aluminum hydroxide on days 1 and 8. From days 15 to 21, and continuing twice weekly for up to 3 weeks, the mice were challenged via intratracheal instillation with 10 μg of OVA (in 50 μl of PBS) (17). The control group was received an equivalent volume of PBS following the same schedule. In the intervention group, CYP (10 mg/kg; cat. no. HY-N0710; MedChemExpress) was administered i.p. 2 h prior to each OVA challenge. To investigate the specific impact of IL-33 on Th9 differentiation during pathogenesis, an additional group of OVA-induced allergic asthmatic mice received an anti-mouse IL-33 antibody (100 μg/mouse; cat. no. PA5-47007; Invitrogen; Thermo Fisher Scientific, Inc.) via i.p. injection. All mice were euthanized 24 h after the final challenge on day 21. Each experimental group consisted of six mice, as detailed in the respective figures and legends.

Humane endpoints (criteria for euthanasia): During the experiment, animal health and well-being were monitored daily by designated personnel. Animals were euthanized immediately if they met any of the following pre-established criteria: a body weight loss exceeding 20% of their initial weight (confirmed by two consecutive measurements); severe respiratory distress, including open-mouth breathing at rest, cyanosis of the lips or extremities, a respiratory rate exceeding 130 breaths per min, or severely irregular breathing; a marked reduction in spontaneous activity, such as a failure to explore a novel environment; or unresponsiveness to mild tactile stimuli, including tail pinching or light touch. Additionally, euthanasia was indicated for a severe hunched posture, piloerection, and lethargy persisting for 24 h without clinical improvement. All abnormal observations were documented in the Animal Health Observation Log, and a veterinarian was consulted to determine if early termination was required.

To ensure animal welfare and optimize pain mitigation, pre-anesthesia and handling protocols were designed to minimize stress and respiratory irritation. A total of 30 min prior to anesthesia induction, mice were acclimated in a quiet environment to eliminate stressful stimuli and avoid rough handling. For the intranasal challenge procedure, mice were anesthetized via intraperitoneal injection of sodium pentobarbital at dosages of (50 mg/kg, via i.p.). Following the procedure, anesthesia was discontinued, and mice were placed on a heating pad to recover. Notably, routine sensitization via intraperitoneal

injections on days 0 and 7 did not require anesthesia, as these were performed by skilled personnel within 30 sec.

All mice were humanely euthanized via an overdose of sodium pentobarbital (150 mg/kg, via i.p.). Following injection, animals were observed continuously for at least 5 min to confirm the simultaneous fulfillment of the following cessation criteria: complete absence of respiration (no chest movement) and absolute loss of the pedal withdrawal reflex. As a secondary, mandatory method of euthanasia to ensure death prior to tissue harvest, bilateral pneumothorax was performed on all animals. Sample collection (for example, lung tissue) was conducted immediately thereafter.

Hematoxylin and eosin (H&E) histology staining. The H&E histopathological staining procedure was performed as previously described (18). In brief, the lung tissues were harvested following euthanasia and fixed in formalin at room temperature for 48 h. The fixed samples were then processed and embedded in paraffin blocks. Sections were cut at a thickness of 5 μm and subjected to H&E staining. A Leica DM4000 light microscope (Leica Microsystems GmbH) was used for observation and image acquisition. A final inflammation index score (S) was applied to quantify peribronchial and perivascular inflammatory cell infiltration. This index S includes two sub-scores: Infiltration severity score (S1) and tissue involvement extent score (S2). The S1 was graded 0-3: 0 (normal), 1 (mild, less than 3 cell layers), 2 (moderate, between 4 to 10 cell layers), and 3 (severe, more than 10 cell layers). The layer was counted by nuclear alignment. The S2 is also defined as grade 0 to 3: 0 (none), 1 (focal, <25% of examined area), 2 (multifocal, between 25-75%), and 3 (diffuse, >75%). The overall final inflammatory index was calculated by multiplying two sub-scores: S=S1 x S2 with a range from 0 to 9.

Periodic acid-Schiff histology staining. The PAS staining was performed to evaluate goblet cell hyperplasia according to a previously described protocol (18). Briefly, the lung tissues were fixed in formalin following euthanasia at room temperature for 48 h. The samples were then processed into paraffin-embedded blocks. Sections of 5-μm thickness were cut and stained following standard PAS procedures. Images were acquired under a Leica DM4000 light microscope (Leica Microsystems GmbH). A total of six randomly selected microscopic fields were analyzed for each sample. The formula (number of goblet cells/total airway epithelial cells) x100% was used to calculate the percentage of goblet cells within the airway epithelium.

Flow cytometry. The flow cytometry protocol was performed as previously described (19,20). Briefly, lung samples were enzymatically digested with Collagenase IV (1 mg/ml, cat. no. 17104019; Gibco; Thermo Fisher Scientific, Inc.) and DNase I (5 mg/ml; cat. no. D5025; MilliporeSigma) in a shaking incubator at 37˚C for 30 min. The cell mixture was then gently filtered through a 200-mesh strainer and centrifuged at 290 x g at 4˚C for 5 min. The cell pellet was suspended in 100 μl of FACS buffer containing 1% serum and stained with appropriate antibodies. Finally, each sample was adjusted to a 200 μl FACS buffer and analyzed by flow cytometry (Cytoflex, Beckman Coulter, Inc.; or NovoCyte, ACEA Bioscience, Inc.).

The following antibodies were used in flow cytometry and western blot analyses: Antibodies obtained from eBioscience; Thermo Fisher Scientific, Inc.: CD45-eFluor 506 (30-F11) (1:400; cat. no. 69-0451-80), CD45-FITC (30-F11) (1:500; cat. no. 11-0451-82), CD11b-FITC (M1/70) (1:400; cat. no. 11-0112-82), CD11c-PE-Cyanine7 (1:200; cat. no. 25-0114-82), major histocompatibility complex class II (MHC-II)-AF700 (I-A/I-E) (1:500; cat. no. 56-5321-82), CD24-PE (M1/69) (1:1,000; cat. no. 12-0242-82), CD64-APC (X54-5/7.1) (1:200; cat. no. 17-0641-82), CD86-SB436 (B7-2) (1:200; cat. no. 62-0862-82), CD86-PE (GL1) (1:500; cat. no. 12-0862-82), CD40-SB436 (1C10) (1:200; cat. no. 62-0401-82), CD40-PE (1C10) (1:500; cat. no. 12-0401-82), CD3-FITC (17A2) (1:1,000; cat. no. 11-0032-82), CD4-AF700 (GK1.5) (1:500; cat. no. 56-0041-82), IL-4-PE-Cyanine7 (1:500; cat. no. 25-7041-82), c-Kit-PE (2B8) (1:1,000; cat. no. 12-1171-82), CD25-PE-Cyanine7 (PC61.5) (1:1,000; cat. no. 25-0251-82), Lineage-FITC (1:20; cat. no. 22-7770-72), SCA-1-PE (D7) (1:500; cat. no. 12-5981-82), FcERI-PE (MAR-1) (1:1,000; cat. no. 12-5898-82), IL-33-PE (1:200; cat. no. MA5-23640), CD90-APC (1:1,000; cat. no. 17-0902-82), CD31-BV421 (1:1,000; cat. no. 404-0311-82) and CD24-SB436 (1:500; cat. no. 62-0242-82). Antibodies purchased from BioLegend, Inc.: Ly6G-PerCP (1A8) (1:500; cat. no. 127616), MHC-II-PerCP (I-A/I-E) (1:1,000; cat. no. 107624), interferon (IFN)-γ-BV421 (1:500; cat. no. 505830), IFN-γ-PE (1:500; cat. no. 505808), IL-9-BV421 (1:1,000; cat. no. 514109), IL-9-PE (1:500; cat. no. 514104) and IL-17A-APC (1:500; cat. no. 506916). Antibodies sourced from BD Pharmingen; BD Biosciences: CD326-RB780 (1:500; cat. no. 568736).

ELISA. Lung homogenates were utilized to quantify cytokine levels via ELISA, according to the manufacturers' instructions and previously described protocols (21). ELISA kits for IL-4 (cat. no. JL20266-96T) and IL-13 (cat. no. JL20247-96T) were purchased from Shanghai Jianglai Industrial Co., Ltd., and the IL-9 kit (cat. no. 88-8092-22) was purchased from Thermo Fisher Scientific, Inc.

Toluidine Blue (TB) staining. Following air-drying, the paraffin-embedded sections were deparaffinized using xylene and a graded alcohol series and then rinsed with distilled water. The sections were then subsequently incubated at 60˚C and stained with 1% TB for 30 min. After staining, the sections were rinsed again with distilled water, dehydrated through a graded alcohol series, and cleared in xylene. Finally, the sections were mounted with neutral gum. Microscopic analysis was performed using a DM4000 Leica light microscope (Leica Microsystems GmbH).

Ex vivo DCs isolation and stimulation. Bone marrow-derived DCs (BMDCs) were generated according to a previously established protocol (22). Briefly, on day 1 of the experiment, bone marrow cells were collected from the femurs and tibias of adult C57BL/6J mice. The cells were cultured in basic RPMI-1640 medium (Hyclone; Cytiva) supplemented with 10% fetal bovine serum (FBS; cat. no. 10091148; Thermo Fisher Scientific, Inc.), 10 mM HEPES (cat. no. 15630080; Thermo Fisher Scientific,

Inc.), 2 mM L-glutamine (cat. no. 25030081; Thermo Fisher Scientific, Inc.), 50 mM 2-mercaptoethanol (cat. no. M3148; MilliporeSigma), 50 U/ml penicillin, and 50 μg/ml streptomycin. The cells were maintained in a humidified atmosphere of 5% CO_2 at 37˚C. On day 2 of the experimental, the recombinant protein IL-4 (10 ng/ml; cat. no. 214-14; PeproTech, Inc.) and granulocyte-macrophage colony-stimulating factor (10 ng/ml; cat. no. 315-03; PeproTech, Inc.) were added to the medium to stimulate the cells. On day 7, the derived BMDCs were treated with OVA (10 μg/ml) in the presence or absence of CYP (100 μM). After 16 h of treatment, the cells were harvested for subsequent analysis.

Total mRNA isolation. The total mRNA isolation (cat. no. RC112-01; Vazyme Biotech Co., Ltd.) was performed following previously described protocol (17). Subsequently, complementary DNA was synthesized using a commercial kit (cat. no. R323-01; Vazyme Biotech Co., Ltd.) according to the manufacturer's instructions. The final products were stored in a freezer for future use.

Reverse-transcription quantitative PCR (RT-qPCR). RT-qPCR was performed on a LightCycler 480 II system (Roche Diagnostics) using a commercial kit (cat. no. Q711-02; Vazyme Biotech Co., Ltd.) according to the previously described protocol (17) and the manufacturer's instructions. The thermal cycling program consisted of an initial denaturation at 95˚C for 10 sec, followed by 40 cycles of amplification (95˚C for 10 sec, 58˚C for 10 sec, 72˚C for 10 sec), and a final elongation step at 65˚C for 1 min. Data were analyzed using the $2^{-\Delta\Delta Cq}$ method (23) with GAPDH as the reference gene. The primer sequences were as follws: GAPDH forward, 5'-ATGCCAGTG AGCTTCCCGTTCAG-3' and reverse, 5'-CATCACTGCCAC CCAGAAGACTG-3'; Il-33 forward, 5'-CTACTGCATGAG ACTCCGTTCTG-3' and reverse, 5'-AGAATCCCGTGGATA GGCAGAG-3'; TNF-α forward, 5'-GGTGCCTATGTCTCA GCCTCTT-3' and reverse, 5'-GCCATAGAACTGATGAGA GGGAG-3'; Ccl17 forward, 5'-CGAGAGTGCTGCCTGGAT TACT-3' and reverse, 5'-GGTCTGCACAGATGAGCTTGC C-3'; jagged canonical Notch ligand 1 (Jag-1) forward, 5'-TGC GTGGTCAATGGAGACTCCT-3' and reverse, 5'-TCGCAC CGATACCAGTTGTCTC-3'; Jag-2 forward, 5'-CGCTGCTAT GACCTGGTCAATG-3' and reverse, 5'-TGTAGGCGTCAC ACTGGAACTC-3'.

Western blotting. The protein expression was determined by western blotting in accordance with previously described protocol (18,20). Samples were lysed in ice cold radio immunoprecipitation assay buffer (cat. no. P0013C; Beyotime Institute of Biotechnology) containing a protease/phosphatase inhibitor cocktail and 5 mm steal beads and then homogenized mechanically. The prepared protein samples were measured with BCA based protein qualification kit (cat. no. P0012; Beyotime Institute of Biotechnology), then were resolved by electrophoresis in 12% SDS-PAGE and then electroblotted onto a microporous polyvinylidene difluoride membrane via wet transfer at a constant current of 200 mA for 2 h. The membrane was blocked with 5% non-fat milk in Tris-buffered saline/Tween (0.05%) for 1 h, followed by incubation with specific primary antibodies overnight at 4˚C. After washing, the membrane was incubated with horseradish peroxidase-conjugated anti-rabbit or anti-mouse secondary antibodies at 4˚C for 2 h. The target bands were visualized using an ECL substrate kit (cat. no. 4AW011-20; Beijing 4A Biotech Co., Ltd.), and images were acquired with a Bio-Rad ChemiDoc Touch imaging system. Data were analyzed using ImageJ 1.47 (National Institutes of Health). Antibodies obtained from Cell Signaling Technology, Inc.: phosphorylated (p-) NF-κB (1:1,000; cat. no. 3033), NF-κB (1:1,000; cat. no. 8242), p-JNK (1:1,000; cat. no. 4668S), JNK (1:1,000; cat. no. 9252S), p-c-Jun (1:1,000; cat. no. 3270S), c-Jun (1:1,000; cat. no. 9165S), p-PAK1 (1:1,000; cat. no. 2606S), PAK1 (1:1,000; cat. no. 2602S), STAT6 (1:1,000; cat. no. 5397S) and p-STAT6 (1:1,000; cat. no. 56554S). Antibodies purchased from Thermo Fisher Scientific, Inc.: STAT5 (1:500; cat. no. 71-2500), p-STAT5 (1:1,000; cat. no. PA5-104895), p38 (1:2,000; cat. no. MA5-41213), p-p38 (1:1,000; cat. no. 44-684G), ERK1/2 (1:1,000; cat. no. 13-6200) and p-ERK1/2 (1:1,000; cat. no. 44-680G). p-PAK1^{Ser144} (1:1,000; cat. no. YM-033315R) antibody was purchased from Shanghai Yunmai Biotechnology Co., Ltd. and GAPDH (1:2,000; cat. no. AF2819) antibody was purchased from Beyotime Institute of Biotechnology. Secondary antibodies: Goat anti-Rabbit IgG (H+L) Secondary Antibody, HRP (1:5,000; cat. no. 31460; Invitrogen; Thermo Fisher Scientific, Inc.). Goat anti-Mouse IgG (H+L) Secondary Antibody, HRP (1:5,000; cat. no. 31430, Invitrogen; Thermo Fisher Scientific, Inc.).

DCs and naïve CD4$^+$ cell co-culture. To investigate whether CYP influences Th2/Th9 differentiation by promoting DC maturation, BMDCs were treated with or without CYP (100 μM) for 2 h and then stimulated with OVA (10 μg/ml) for an additional 16 h. Subsequently, 1.5x10^5 BMDCs were co-cultured with 3x10^5 naïve CD4$^+$ T cells (isolated from the spleens of OT-II mice) in 96-well plates. After 3 days of culture, the cells were stimulated for 6 h with 1x cocktail reagent to activate cells (cat. no. 423303; BioLegend, Inc.; 500x including PMA 40.5 μM, Ionomycin 669.3 μM and brefeldin A 2.5 mg/ml) prior to flow cytometric analysis. Intracellular staining for IFN-γ and IL-4 was performed to evaluate Th1 and Th2 differentiation, respectively.

To investigate whether CYP regulates Th9 cell differentiation by modulating DC maturation, BMDCs were treated with or without CYP for 2 h, followed by stimulation with OVA for an additional 16 h. Subsequently, the treated BMDCs were co-cultured in 96-well plates with naïve CD4$^+$ T cells isolated from spleen in the presence of 8 ng/ml of TGF-β (cat. no. 7754-BH-005/CF; R&D Systems, Inc.) for up to 3 days. To assess Th9 differentiation, the cells were stimulated with a 1x cocktail reagent to activate cell for the final 6 h of culture, and intracellular IL-9 expression levels were analyzed.

Th2/Th9 cells in vitro differentiation. T cell differentiation was performed according to an established protocol (24). Briefly, the naïve CD4$^+$ T cells were isolated from mice spleen using a CD4$^+$ T cell isolation kit (cat. no. 19852; Stemcell Technologies, Inc.). The cells were seeded onto plates coated with anti-CD3 (2 μg/ml; cat. no. 100340; BioLegend, Inc.) and anti-CD28 (2 μg/ml; cat. no. 102116; BioLegend, Inc.) at a density of ~100,000 cells/well. The T cell polarization was

induced with specific cytokines and/or antibodies as follows: for Th2 conditions, IL-4 (20 ng/ml; cat. no. 214-14; PeproTech, Inc.) and IL-2 (100 U/ml; cat. no. 575406; BioLegend, Inc.); for Th9 conditions, IL-4 (20 ng/ml), recombinant human TGF-β (8 ng/ml), IL-2 (100 U/ml) and anti-IFN-γ (50 μg/ml; cat. no. BE0055; BioXCell). The cells were cultured at 37˚C and 5% CO_2 in RPMI 1640 (Hyclone; Cytiva) with 10% heat inactivated FBS for 48 h prior to flow cytometric analysis (Cytoflex, Beckman Coulter, Inc.; NovoCyte, ACEA Bioscience, Inc.).

To further investigate how CYP and IL-33 affect Th2/Th9 differentiation, cells were cultured under differentiation conditions in the presence or absence of CYP (100 μM) or IL-33 (20 ng/ml; cat. no. 210-33; PeproTech, Inc.) or their combinations.

Molecule and protein docking energy analysis. Initial structural information for PAK1 was obtained from the UniProt database (O88643_PAK1_MOUSE; https://www.uniprot.org/uniprotkb/O88643/entry) and processed using AutoDock Tools 1.5.7; (http://mgltools.scripps.edu/). Similarly, the structure of CYP was established using Materials Studio and AutoDock Tools 1.5.7. AutoDock 4.2.6 (https://autodock.scripps.edu/) was used for docking analysis. Images of PAK1 and CYP interaction were generated by PyMOL 2.5.5 (https://www.pymol.org/dokuwiki/) and LigPlot+ 2.2.8 (https://www.ebi.ac.uk/thornton-srv/software/LigPlus/).

Expression and purification of PAK1 (S144A) mutant protein. The pET22b vector was used to construct the pET22b-PAK1 (S144A) plasmid. *E. coli* BL21 (DE3) competent cells were transformed to express PAK1 (S144A) protein. After purification with nickel column affinity chromatography, the molecular weights of the proteins were verified by SDS-PAGE.

Biacore surface plasmon resonance (25) analyzes CYP interacts with PAK1. The interaction of CYP with wild-type PAK1 (cat. no. HY-P71530; MedChemExpress) or its mutant PAK1 (S144A) was analyzed using a Biacore 8000 system (Cytiva) with a CM5 sensor chip (cat. no. BR-1005-30; Cytiva). In brief, flow channel 2 and channel 4 were activated at a flow rate of 10 μl/min using a 1:1 mixture of 1-ethyl-3-(3-dimethylaminopropyl) carbodiimide (EDC; Cytiva) and N-hydroxy-succinimide (Cytiva) from an amine coupling kit (cat. no. BR100050; Cytiva). The ligand protein was diluted with sodium acetate buffer (cat. no. BR100349; Cytiva) to 50 μg/ml. PAK1 protein was immobilized on channel 2 at a flow rate of 10 μl/min, and PAK1 (S144A) protein was immobilized on channel 4 at the same flow rate. The coupling curve was recording in real-time. And the Biacore Insight evaluation software (Cytiva) was used to analyze binding kinetics and fit the data to a 1:1 Langmuir binding model.

Homogeneous time-resolved fluorescence (HTRF) assay. CYP inhibits PAK1 kinase activity was tested using HTRF assay. The HTRF KinEASW STK S1 kit (cat. no. 62ST1PEJ; Revvity, Inc.) was used to test whether CYP inhibits PAK1 kinase activity. The procedure was performed following the manufacturer's instruction. Briefly, 100 nl of CYP (2 mM) was mixed with 5 μl of 2x PAK1 kinase solution and incubated for 10 min at 25˚C. Then, 5 μl of 2x ATP substrate solution was added and incubated for 60 min at 25˚C. After that, another 10 μl of 2x kinase test reagent was added and incubated for additional 40 min, followed by recording of the fluorescence signals at 620 and 665 nm using a plate reader (PHERAstar FSX; BMG Labtech). The percent inhibition (% inh) for compound well=100x (average High control-compound well)/(average High control-average Low control).

Statistical analysis. Data are presented as the mean ± standard deviation and were analyzed using GraphPad Prism 9 (Dotmatics). Statistical comparisons between two groups were performed using an unpaired Student's t-test. For multiple group comparisons, a one-way analysis of variance (one-way ANOVA) followed by Tukey's test for multiple comparisons was performed. Statistically significant difference was defined as $P<0.05$.

Results

CYP attenuates OVA-induced allergic inflammation and DC maturation. Mice exposed to OVA can develop the bronchial airway hyper-response resulting asthma. In the present study, it was found that mice treated with a combination of OVA and CYP exhibited significantly decreased inflammation compared with mice treated with OVA alone (Fig. 1A and B). Additionally, a significantly higher level of goblet cells was observed in the airway lung tissue of the OVA-treated group vs. to the PBS control group; however, CYP treatment successfully attenuated this increase (Fig. 1C and D). By contrast, the addition of CYP did not significantly suppress the elevated number of neutrophils (Neu) induced by OVA (Fig. 1E and F). The results further indicate that the numbers of both eosinophils (Eos) and DCs were significantly increased in the OVA group relative to the PBS control but were markedly decreased in the OVA plus CYP group compared with the OVA-alone group (Fig. 1G). Similar suppressive effects of CYP were observed regarding lung macrophages and B cells; the number of macrophage (MΦ) (Fig. S1A and B) and B cells (Fig. S1C) rose following OVA exposure but dropped sharply with addition of CYP. Furthermore, the OVA-triggered elevations in $CD86^+$ and $CD40^+$ DCs in the mouse lungs were significantly declined by CYP treatment (Fig. 1H).

Taken together, these findings demonstrate that CYP attenuates OVA-induced lung inflammation and goblet cell hyperplasia. Furthermore, CYP reduces the accumulation of Eos, DCs, and $CD86^+$ and $CD40^+$ DCs triggered by OVA, while exerting no detecw effects on Neu.

CYP attenuates OVA-induced Th2/Th9 immune responses in vivo. Furthermore, it was found that OVA challenge significantly increased the absolute the numbers of Th2 and Th9 cells in mice lung tissues (Fig. 2A-C). While OVA exposure also elevated Th17 cell counts, this increase did not reach statistical difference compared with PBS control group. Notably, the Th1 cell numbers remained unresponsive to OVA treatment. Conversely, administration of CYP in combination with OVA significantly reduced the numbers of Th2/Th9 cells compared with OVA-alone group. Consistent with these findings, the percentages of Th2/Th9/Th17 cells, but not Th1 cells, were elevated by OVA and subsequently suppressed upon CYP

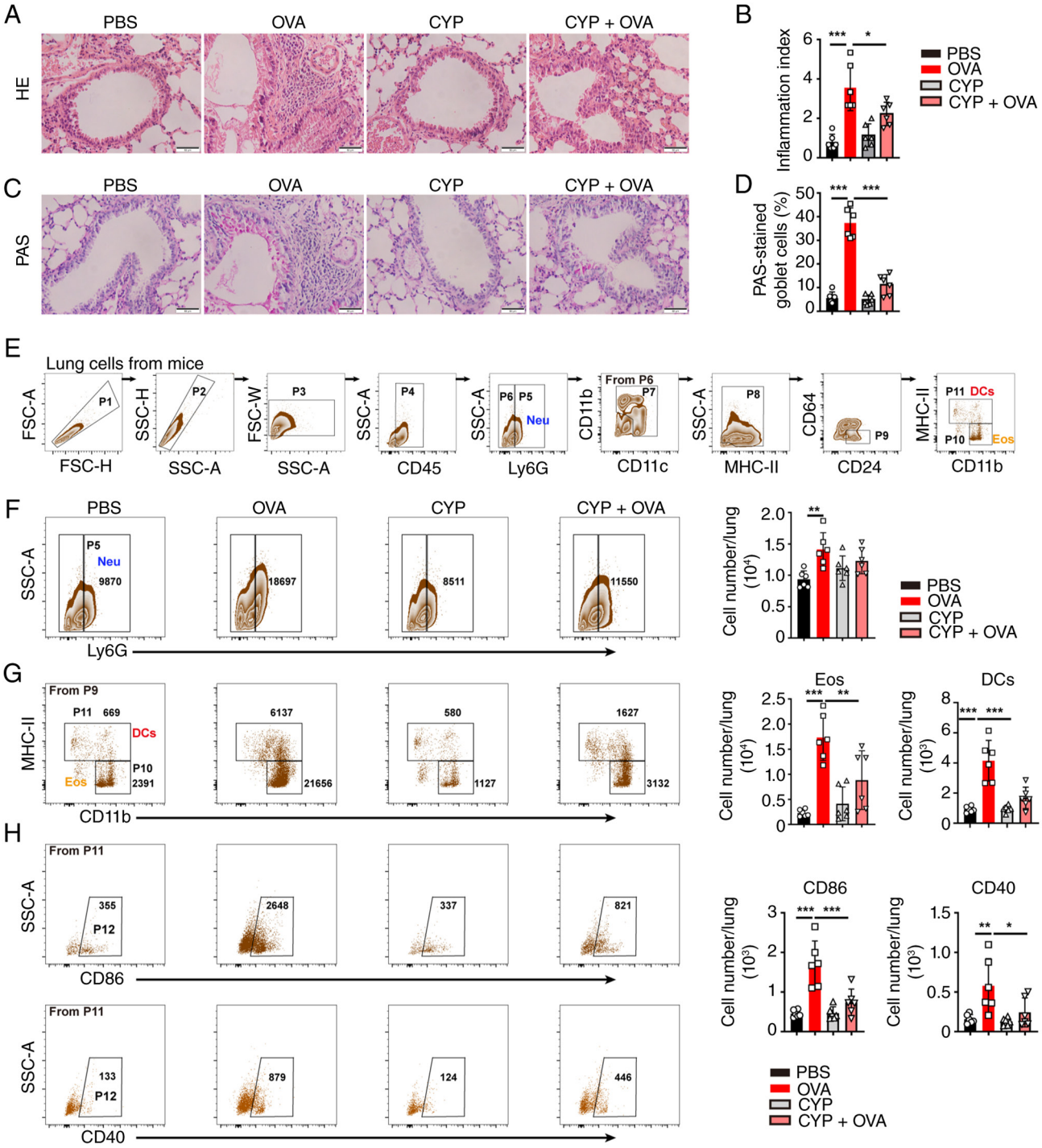

Figure 1. CYP attenuates OVA-induced allergic inflammation and dendritic cell maturation. (A and B) H&E-stained and (C and D) PAS-stained lung tissue sections from the indicated treatment groups in an asthmatic mouse model. Inflammation index and the percentage of goblet cell were quantified across six randomly selected fields per section. (E) Gating strategy used for the flow cytometry analysis of pulmonary immune cell populations (F and G) Quantification of distinct immune cell subsets, identified as: (F) Neu (Ly6G$^+$ Neu from P4); (G) Eos (MHC-II^{low}CD11b$^+$ Eos from P9) and DCs (MHC-II^{high} DC from P9). (H) Flow cytometric analysis of mature CD86$^+$ and CD40$^+$ DCs in the lungs of asthmatic mice. Data are shown as the mean ± standard deviation (n=6). *P<0.05, **P<0.01 and ***P<0.001 were obtained by one-way ANOVA followed post calculation. CYP, α-Cyperone; OVA, ovalbumin; Neu, neutrophils; Eos, eosinophils; DCs, dendritic cells; MHC-II, major histocompatibility complex class II; PAS, periodic acid-Schiff.

treatment (Fig. 2D). Finally, evaluation of specific cytokines in lung tissue homogenates revealed that Il-4, Il-13 and Il-9 levels were upregulated by OVA challenge, an effect that was effectively reversed by CYP co-treatment (Fig. 2E).

The effects on the MLN of the mice were next evaluated. OVA challenge induced a robust enlargement of the MLNs compared with the PBS control; however, the addition of CYP significantly attenuated this increase in size (Fig. 3A). Flow cytometric analysis revealed that the numbers of CD86$^+$ and CD40$^+$ DCs within the MLNs peaked in the OVA-treated group, whereas CYP treatment significantly lowered these levels (Fig. 3B). Furthermore, the absolute numbers of Th2/Th9/Th17 helper T-cell subsets were significantly increased in the MLN samples of OVA-treated mice, an effect that was significantly

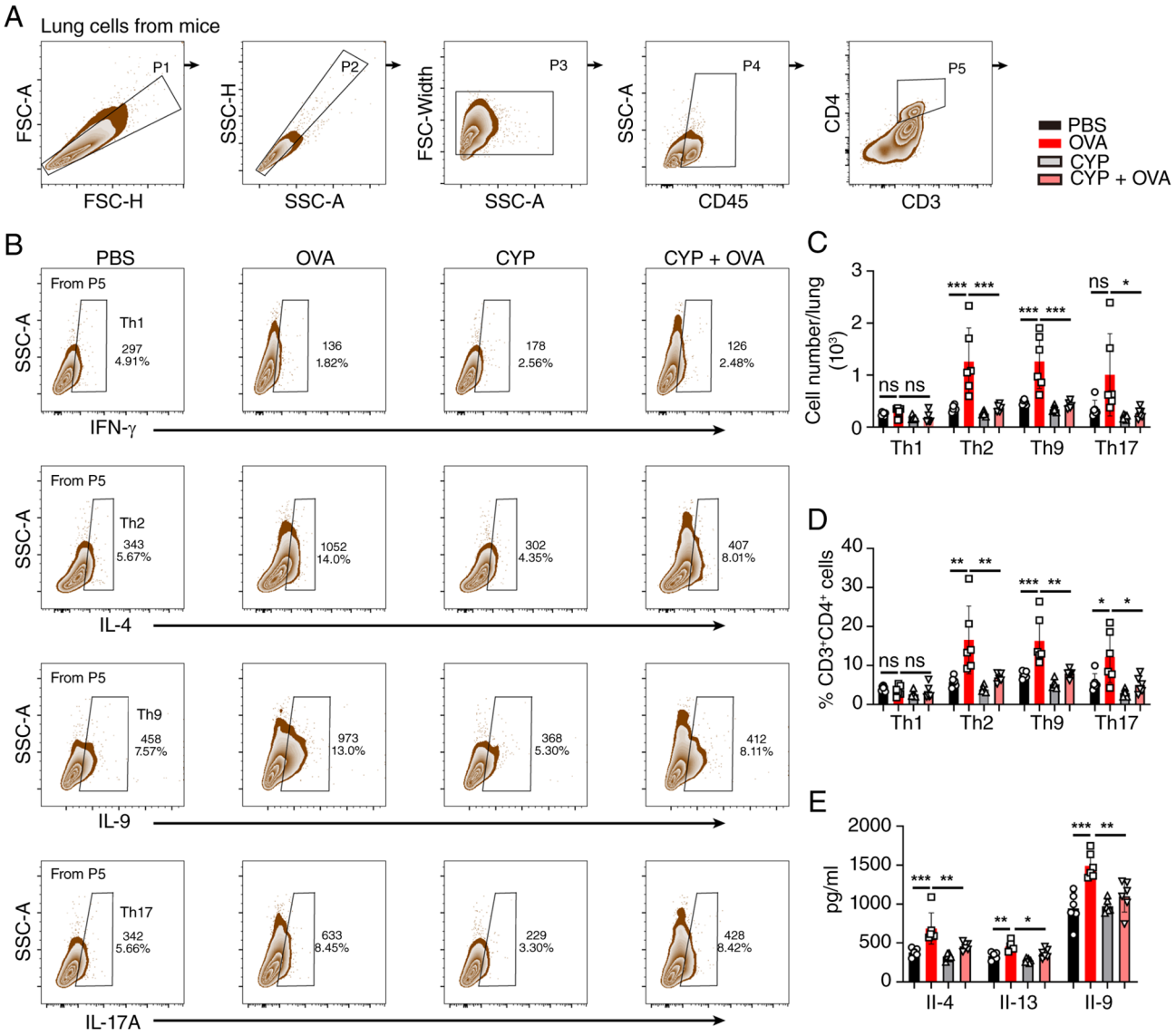

Figure 2. CYP suppresses OVA-induced Th2/Th9 immune responses *in vivo* without affecting Th1 responses. (A) Flow cytometric analysis of T cell subsets isolated from the lung tissue of mice across the indicated experimental groups. The primary gating strategy was defined as: P5 $CD45^+CD4^+CD3^+$. (B) Representative gating analysis within the P5 $CD45^+CD4^+CD3^+$ population to identify IFN-γ^+ Th1, IL-4^+ Th2, IL-9^+ Th9 and IL-$17A^+$ Th17 cells. (C) Absolute cell numbers of Th1/Th2/Th9/Th17 subsets in lung tissue. (D) Percentages of Th1/Th2/Th9/Th17 cells relative to the total $CD4^+CD3^+$ T cell populations. (E) ELISA quantification of Il-4, Il-13 and Il-9 levels in mouse lung homogenates. Data are shown as the mean ± standard deviation (n=6). *P<0.05, **P<0.01 and ***P<0.001 were calculated by one-way ANOVA followed post comparison. CYP, α-Cyperone; OVA, ovalbumin.

reversed by CYP administration (Fig. 3C and D). These findings were consistently recapitulated in the corresponding percentage frequencies of Th2/Th9/Th17 cells (Fig. 3E).

These results suggest that while Th2/Th9 cells mediate the immune responses to OVA exposure in allergic asthmatic mice, Th1 cells do not. Furthermore, CYP demonstrates a protective effect against OVA-triggered allergic responses.

CYP suppresses OVA-induced immune responses in mast cells and ILC2 cells. Furthermore, it was observed that the number of lung mast cells significantly increased following OVA treatment and subsequently decreased with addition of CYP; however, basophil numbers remained unaffected (Figs. S2A and B; 4A). Similarly, group 2 innate lymphoid cells (ILC2) exhibited a respond pattern comparable to that of mast cells under both CYP and OVA treatments (Figs. S1 and 4B). Histology staining further confirmed the responsiveness of lung mast cells to OVA and CYP exposure (Fig. 4C). Taken together, these results indicate that CYP selectively suppresses OVA-induced mast cells and ILC2 immune responses instead of basophils.

CYP attenuates OVA-induced DCs' immune responses via the PAK1-JNK/NF-κB signaling. DCs were significantly activated by OVA shown as enhanced percentages of $CD40^+$, $CD86^+$ and MHC-II^+ of cells within $CD11c^+$ population (Fig. 5A and B). Conversely, the addition of CYP suppressed this DC maturation. Consistent with previous findings confirming OVA-induced DC activation and maturation, OVA treatment significantly upregulated the mRNA expression levels of Il-33, TNFα, Ccl17 and Jag-1, whereas Jag-2 expression remained unchanged. However, this elevated expression

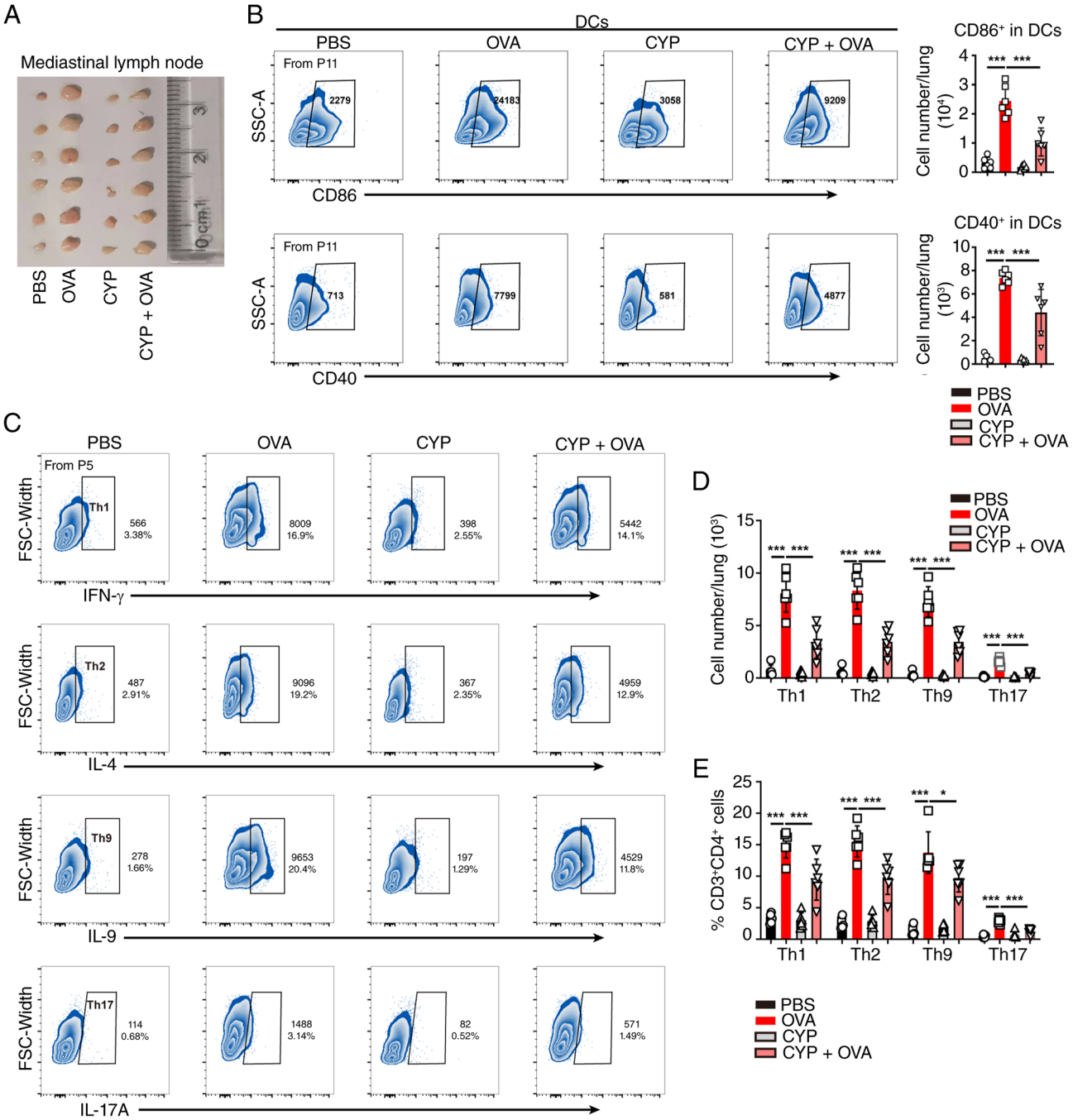

Figure 3. CYP attenuates OVA-induced DC maturation and Th2/Th9 differentiation in the MLNs of asthmatic mouse. (A) Representative images showing MLN size across the experimental groups. (B) Flow cytometry quantification of $CD86^+$ and $CD40^+$ DCs isolated from the MLN of mice in the PBS, OVA, CYP and CYP + OVA groups. (C) Gating strategy (P5) for the analysis of IFN-γ^+ Th1, IL-4^+ Th2, IL-9^+ Th9 and IL-$17A^+$ Th17 cell populations. (D) Absolute cell counts of Th1/Th2/Th9/Th17 subsets within MLN tissue. (E) Percentage of Th1/Th2/Th9/Th17 cell subsets relative to total $CD4^+CD3^+$ T cells. Data are shown as the mean ± standard deviation (n=6). $^*P<0.05$ and $^{***}P<0.001$ were obtained by one-way ANOVA followed post analysis. CYP, α-Cyperone; OVA, ovalbumin; DCs, dendritic cells; MLN, mediastinal lymph node.

of Il-33, TNFα, Ccl17 and Jag-1 was significantly reduced in the CYP and OVA co-treatment group (Fig. 5C). Given that the STAT/p38/ERK and JNK/NF-κB pathways are associated with asthma pathogenesis (22,26,27), these downstream signaling mechanisms were next evaluated via western blotting. The activation of the STAT5/6, p38 and ERK1/2 pathways did not alter substantially under OVA exposure regardless of CYP co-treatment (Fig. S3). By contrast, in-depth analysis indicated that OVA stimulation robustly activated the p-PAK1, p-JNK, p-c-Jun and p-NF-κB signaling networks, and these elevated phosphorylation levels were sharply attenuated upon addition of CYP (Fig. 5D).

To investigate whether CYP modulates T cell differentiation by altering OVA-triggered DC maturation, OVA pre-treated DCs were co-cultured with naïve $CD4^+$ T cells isolated from OT-II mice (Fig. 5E). Upon OVA stimulation, the percentage of $CD4^+$IL-4^+ T cells significantly increased. However, this upregulation was effectively suppressed in the OVA plus CYP group, which showed only a marginal increase compared with PBS group (Fig. 5F). Furthermore, when exogenous TGF-β1

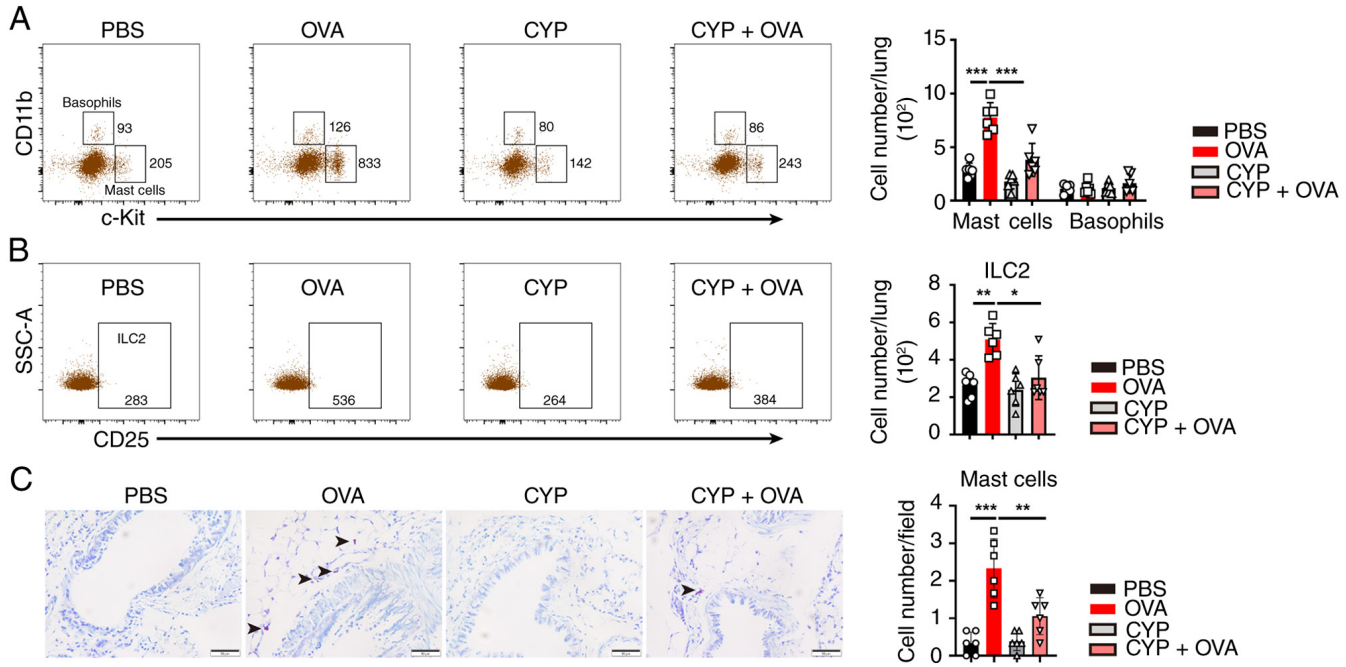

Figure 4. CYP suppresses OVA-induced mast cells and ILC2 immune responses. (A) Flow cytometry analysis of basophils (Lineage$^-$FcERI$^+$CD11b$^+$c-Kit$^-$) and mast cells (Lineage$^-$FcERI$^+$CD11b$^-$c-Kit$^+$) in mouse lung tissue. (B) Flow cytometry quantification of ILC2 (Lineage$^-$c-Kit$^-$SCA-1$^+$CD25$^+$) in mice lung tissue. (C) Representative images and quantification of mast cell staining in lung tissue sections. Data are presented as the mean ± standard deviation (n=6). *P<0.05, **P<0.01 and ***P<0.001 was determined by one-way ANOVA followed by a post-multiple comparison between the two groups. CYP, α-Cyperone; OVA, ovalbumin; ILC2, group 2 innate lymphoid cells.

was added to the co-cultures, the percentage of CD4$^+$IL-9$^+$ T cells increased sharply in the OVA-treated DC group, but this effect was significantly attenuated in the group treated with the combination of OVA and CYP (Fig. 5G).

These results suggest that OVA promotes DC maturation and activation via the PAK1-JNK/NF-κB signaling, which subsequently enhances the differentiation of Th2 (CD4$^+$IL-4$^+$) and Th9 (CD4$^+$IL-9$^+$) cells. Conversely, CYP attenuates DC maturation and activation by inhibiting this same signaling cascade, thereby suppressing Th2/Th9 differentiation.

CYP suppresses IL-33-enhanced Th2 and Th9 phenotype via inhibition of PAK1-JNK/NF-κB signaling. IL-33 is associated with Th2 and Th9 differentiation (28). The present findings indicated that OVA promote IL-33 secretion by DCs. Furthermore, in an OVA-induced asthmatic mice model, the frequencies of IL-33 positive macrophages (Fig. S1D) and DCs (Fig. S1F) were significantly increased following OVA exposure compared with the PBS control group. Conversely, the numbers of IL-33$^+$ Macrophages (MΦ) and DCs were markedly lower in the OVA plus CYP treatment group. Consistent with these findings, the mean fluorescence intensity of IL-33 in MΦ (Fig. S1E), DCs (Fig. S1G) and epithelial cells (Fig. S1H and I) were notably elevated by OVA, an effect that was effectively abrogated by CYP co-administration. Interestingly, no significant changes were observed in either endothelial cells or fibroblast (Fig. S1H and I). To investigate whether CYP modulates Th2/Th9 differentiation, CYP was co-treated alongside IL-33 stimulation. The results of the present study indicated that CYP suppresses IL-33-enhanced Th2 differentiation (Fig. 6A and B). Mechanistically, it was confirmed that IL-33 stimulation activates the p-PAK1, p-JNK, p-c-Jun and p-NF-κB signaling networks; however, these phosphorylation levels were sharply attenuated upon CYP administration (Fig. 6C). Similarly, CYP inhibited IL-33-enhanced Th9 differentiation (Fig. 6D and E), a process concurrently regulated by the activated PAK1-JNK/NF-κB signaling networks (Fig. 6F).

To further investigate whether IL-33 modulates Th9 differentiation during OVA-induced asthma pathogenesis, an anti-IL-33 antibody was used to deplete IL-33 *in vivo*. The results indicated that IL-33 depletion attenuated OVA-induced lung inflammation (Fig. S4A-D). Specifically, OVA-induced increases in Neu, MΦ, B cells, Eos, DCs, CD86$^+$ DC cells and mast cells were significantly reduced following IL-33 depletion; whereas basophils counts remained unchanged (Fig. S4E-J). Notably, anti-IL-33 treatment specifically targeted Th2/Th9 subtypes, which significantly plummeted, while Th1/Th17 populations did not show comparable changes (Figs. S4 and S5). Collectively, these results indicated that CYP suppresses IL-33-triggered Th2 and Th9 differentiation via PAK1-JNK/NF-κB signaling.

CYP inhibits PAK1 activity by blocking phosphorylation at Ser144 site. Computational analysis was performed to further evaluate potential interaction between CYP and PAK1. The docking score/binding energy threshold value was set as -5 kcal/mol. The value below -5 kcal/mol is considered relatively strong affinity (29). The results indicate that CYP directly interacts with PAK1 at residues PAK1-Lys141 and PAK1-Ser144. Notably, the interaction at PAK1-Ser144 exhibited the lowest docking energy of -5.27 kal/mol, suggesting the strongest binding conformation (Figs. 7A and S6A-C). Previous studies have established that multiple phosphorylation sites

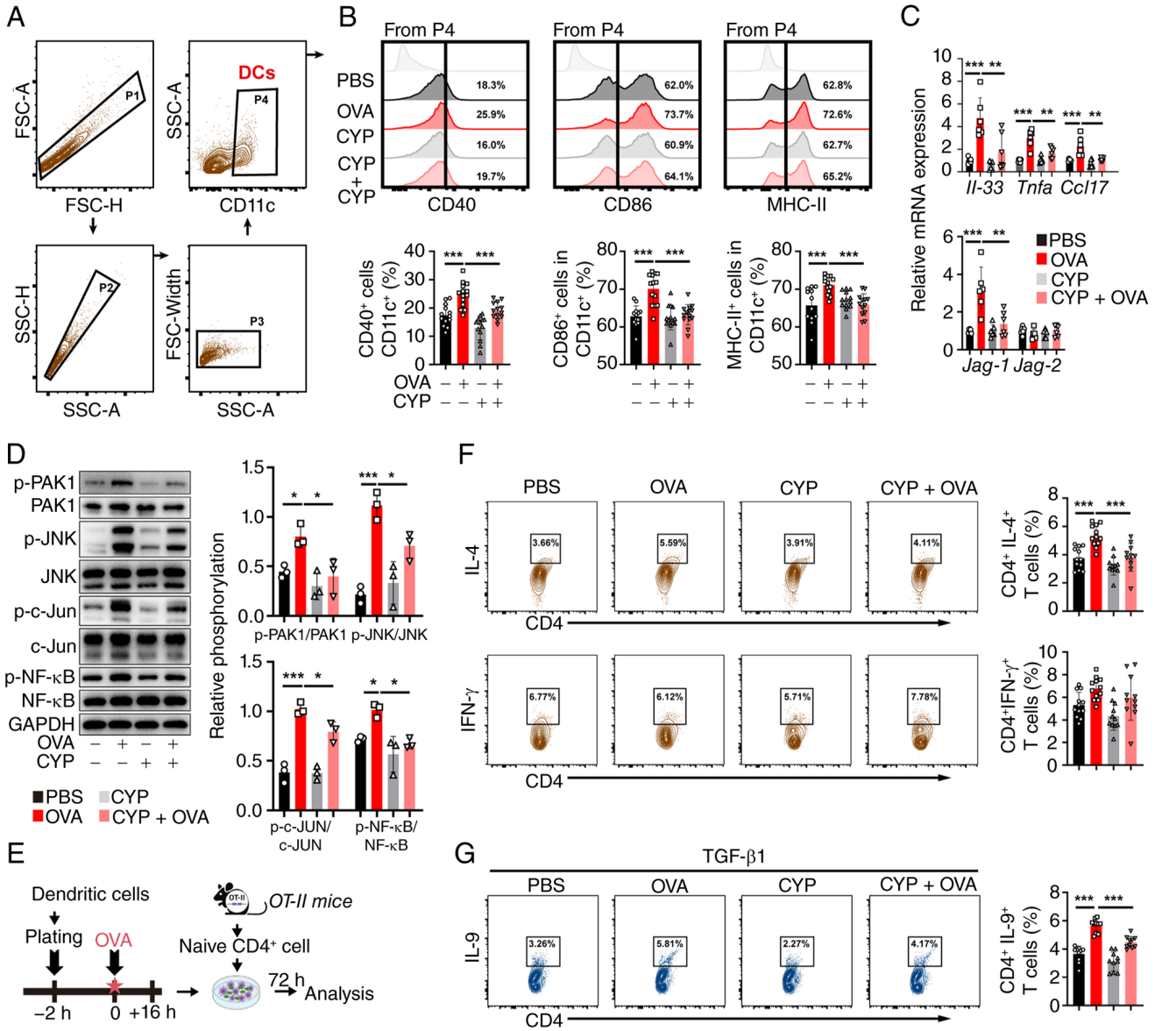

Figure 5. CYP attenuates OVA induced immune responses in DCs via PAK-JNK/NF-κB pathway. (A) Schematic representation of the flow cytometry gating strategy for BMDCs (CD11c$^+$). (B) Flow cytometry analysis of CD40, CD86 and MHC-II expression on OVA-exposed DCs treated with or without CYP. (C) Reverse transcription-quantitative PCR analysis of Il-33, TNFα, Ccl17, Jag-1 and Jag-2 mRNA expression levels. (D) Western blot analysis of PAK, JNK, c-Jun and NF-κB signaling components in DCs. (E) Experimental workflow for the *in vitro* co-culture of BMDCs and naïve CD4$^+$ T cells. (F and G) Flow cytometry analysis of (F) CD4$^+$IL-4$^+$ and CD4$^+$IFN-γ$^+$, and (G) CD4$^+$IL-9$^+$ T cell populations within the BMDCs and CD4$^+$ T cell co-culture system. The results are shown as the mean ± standard deviation (n=6). *P<0.05, **P<0.01 and ***P<0.001 were calculated by one-way ANOVA followed by post comparison. CYP, α-Cyperone; OVA, ovalbumin; DCs, dendritic cells; BMDCs, bone marrow DCs; p-, phosphorylated; Jag-1, jagged canonical Notch ligand; NF-κB, nuclear factor-κB.

are critical for PAK1 activation, such as PAK1-Ser144 and PAK1-Thr423 (30,31). To further verify that PAK1-Ser144 is a critical binding cite for CYP, PAK1 (S144A) mutant protein was generated and its binding affinity for the CYP was compared against wildtype PAK1. Notably, with a 10-fold higher concentration of CYP was required to achieve interaction with the PAK1 (S144A) mutant compared with the wildtype PAK1. Kinetic analysis revealed that CYP binds to wild-type PAK1 4.1-fold faster than binds to PAK1 (S144A) mutant, while the dissociation rate from PAK1 (S144A) is 4.3-fold quicker than PAK1. Ultimately, CYP showed a 17.2-fold stronger affinity of PAK1 than the mutant form PAK1 (S144A) (Fig. 7B and C). Consistent with these findings, a HTRF assay determined the half-maximal inhibitory concentration of CYP in PAK1 is 96.88 μM (Fig. 7D). Also, the western blot result indicated that OVA stimulation enhances phosphorylation of PAK1 (Ser-144) in DCs; the effect was markedly attenuated by the additional CYP (Fig. 7E). Similarly, IL-33 could promote phosphorylation of PAK1 (Ser-144) in both Th2 and Th9 but no significant difference was observed when CYP was added compared with control group (Fig. 7E). These results indicate that CYP interacts with PAK1-Ser144, blocking its phosphorylation and subsequently suppressing the PAK1-JNK/NF-κB signaling networks.

Collectively, OVA activated PAK1, which subsequently triggers the JNK-c-Jun/NF-κB signaling. This cascade promotes DCs maturation by enhancing MHC-II, CD86 and CD40 overexpression, while concurrently stimulating IL-33 release. In turn, IL-33 enhances the differentiation of Th2/Th9

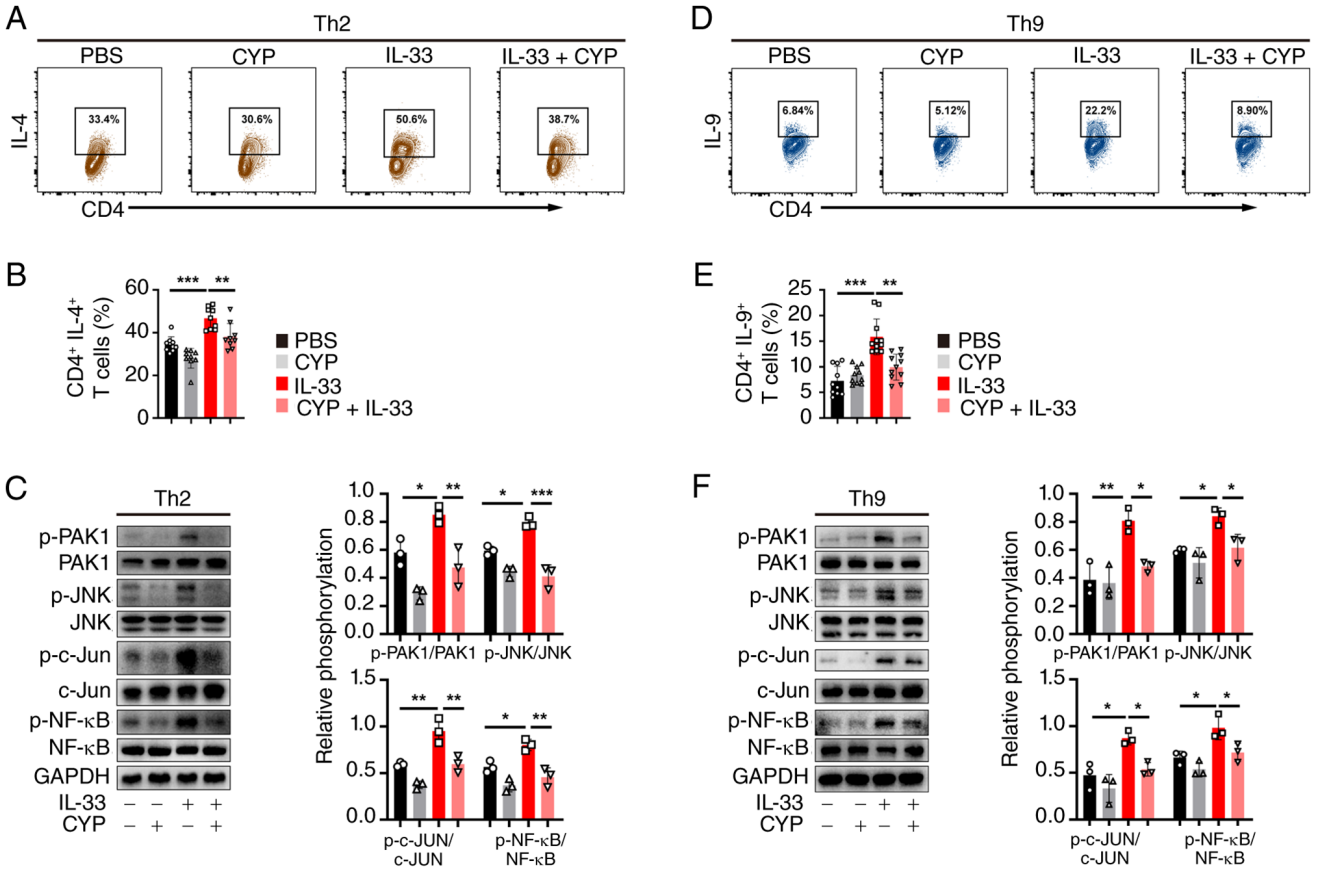

Figure 6. CYP targets PAK1-JNK/NF-κB signaling to modulate IL-33 enhanced Th2 and Th9 differentiation. (A and B) Flow cytometric analysis of CYP-modulated Th2 differentiation in the presence or absence of IL-33 stimulation. (C) Western blot analysis and qualification of CYP modulating the Th2 phenotype via NF-κB, c-Jun and PAK1 signaling; (D and E) Flow cytometric analysis of CYP-modulated Th9 differentiation in the presence or absence of IL-33 stimulation. (F) Western blot analysis and qualification of CYP modulating the Th9 phenotype via NF-κB, c-Jun and PAK1 signaling. Data are shown as the mean ± standard deviation (n≥3). *P<0.05, **P<0.01 and ***P<0.001 was obtained by one-way ANOVA followed post analysis. CYP, α-Cyperone; NF-κB, nuclear factor-κB; c-Jun, c-Jun N-terminal kinase (JNK)-mediated activated protein-1; p-, phosphorylated.

cells by activating their intrinsic PAK1/JNK-c-Jun/NF-κB signaling networks. Conversely, CYP directly binds to PAK1 at S144 site to inhibit its kinase activity, thereby suppressing both OVA-induced DCs maturation and IL-33-mediated Th2/Th9 differentiation.

Discussion

Allergic asthma is a chronic inflammatory disorder characterized by elevated IgE production and the extensive recruitment of mast cells and Eos. While this pathology is primarily driven by Th2-type immune responses (32), and Th9 cells have also been identified as critical mediator of the disease (33). Macrophage (IL-33 + IL-2) significantly enhance OVA-triggered JAK2-STAT3-IRF1 pathway-dependent allergic airway inflammatory pathogenesis (34). In the present study, it was demonstrated that the inflammatory inhibitor CYP effectively attenuates airway inflammation and mucus hypersecretion in an OVA-mediated murine model of allergic asthma. These effects were associated with a significant reduction in the proportions of mature DCs and Th2/Th9 cells within lung tissue and MLNs (Figs. 1 and 2). Furthermore, in mouse BMDCs, CYP treatment inhibited the OVA-induced expression of CD40, CD86 and MHC-II (Fig. 5). Given that OVA-enhanced DCs' maturation promotes the differentiation of Th2/Th9 lineages (Fig. 5), the present findings suggest that CYP alleviates allergic asthma by suppressing DC maturation, thereby limiting subsequent Th2/Th9 cell differentiation.

DCs' maturation is governed by regulatory networks involving key transcription factors, such as STATs, ERK1/2, p38, NF-κB, JNK and c-Jun (35-38). The activation of ERK1/2, NF-κB and JNK pathways is closely associated with PAK1 (39-41). Furthermore, PAK1 has been shown to regulate both STAT5 (42) and p38 (43) signaling. In the present study, it was demonstrated that while OVA promotes PAK1 phosphorylation, whereas CYP effectively inhibits both OVA-induced PAK1 activation and the subsequent phosphorylation of JNK, c-Jun, and NF-κB in DCs (Fig. 5). However, the STAT5/6, p38 and ERK1/2 signaling did not notably change (Fig. S3). Given that PAK1 is closely linked to the JNK-c-Jun/NF-κB signal networks that drive inflammatory progression (44-46), these data suggest that CYP may modulate maturation of DCs through this pathway. The molecular docking analysis (Fig. 6) further revealed that CYP bind to the serine 144 (Ser144) residue of the PAK1 protein. Because phosphorylation at the serine141 and/or Ser144 sites is essential for PAK1 kinase activity, the following assays were performed to confirm this. The SPR and kinase activity assay results revealed that CYP binds at PAK1^{Ser144} sterically hinders phosphorylation at this critical site. In the context of allergic asthma, the present results

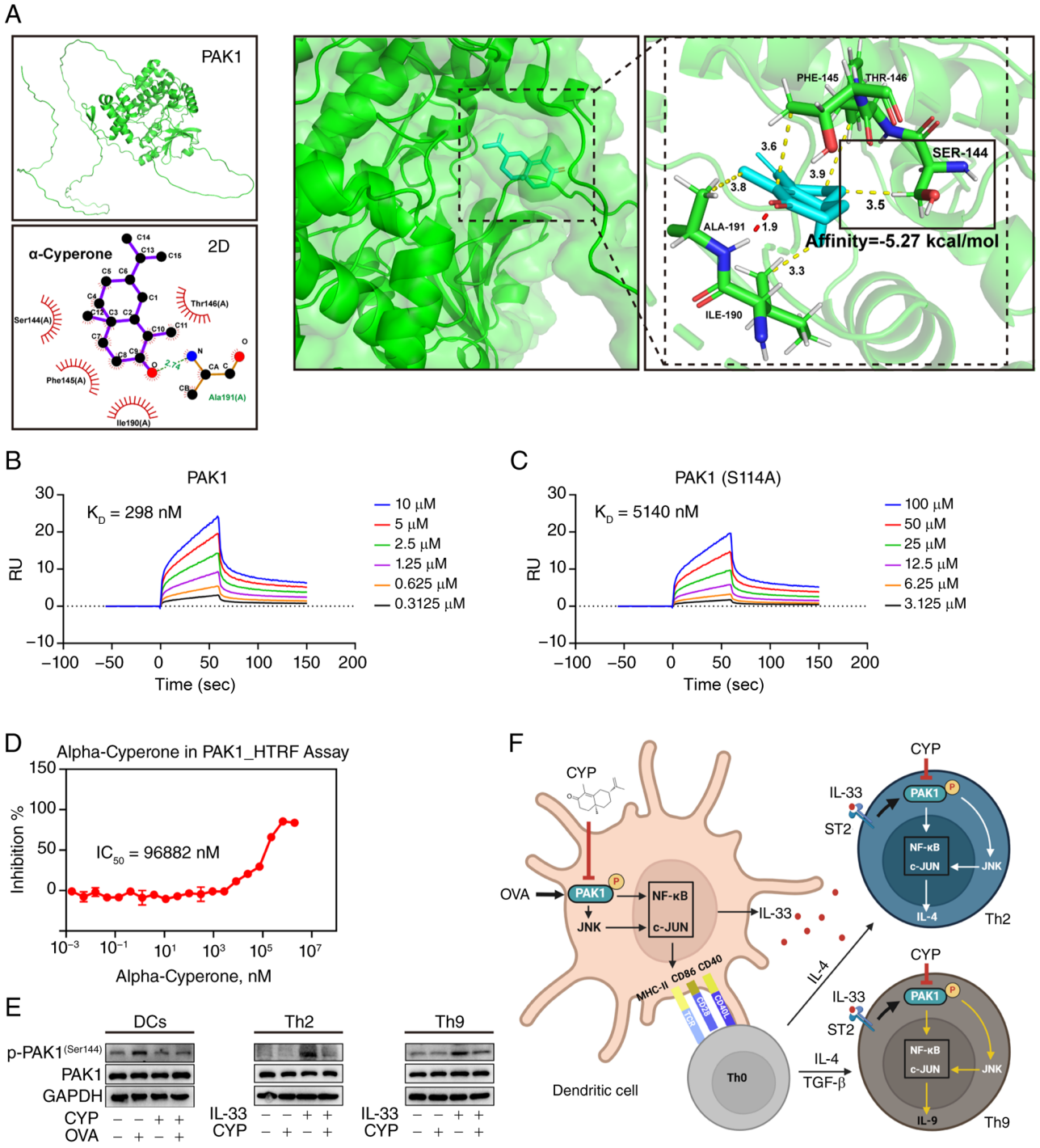

Figure 7. CYP suppresses PAK1 activation by inhibiting Ser144 phosphorylation. (A) Computational docking analysis of CYP docking with PAK1 protein. (B and C) Biacore surface plasmon resonance analysis of the interaction between CYP and wildtype PAK1 (B) or the mutant PAK1 (S144A) (C). Note: A presents Human PAK1 while B presents Human PAK1 (S144A) mutant form. (D) Homogeneous time-resolved fluorescence assay assessing the inhibitory effect of CYP on PAK1 activity. (E) Western blot analysis of p-PAK1^{Ser144}/PAK1 expression in DCs, Th2 and Th9 cells stimulated with OVA or IL-33 with/without CYP treatment. (F) Schematic diagram summarizing the underlying mechanisms: CYP attenuates dendritic cell maturation and IL-33 secretion by blocking the PAK1-JNK/NF-κB signaling, thereby suppressing Th2/Th9 differentiation. Concurrently, CYP directly inhibits naïve T cell differentiation into Th2/Th9 cells by blocking the IL-33 activated PAK1-JNK/NF-κB pathway. Overall, CYP alleviates OVA-induced allergic inflammation by targeting PAK1 to inhibit PAK1-JNK/NF-κB axis. CYP, α-Cyperone; K_D, dissociation constant (lower value indicates stronger affinity) K_a, association rate constant (higher value indicates faster binding) K_d, dissociation rate constant (higher value indicates quicker dissociation); DCs, dendritic cells; OVA, ovalbumin; NF-κB, nuclear factor-κB; c-Jun, c-Jun N-terminal kinase (JNK)-mediated activated protein-1.

suggest that PAK1 activates the JNK-c-Jun/NF-κB signaling pathway to facilitate DCs maturation. Furthermore, data from DCs' and CD4$^+$ T cells' co-culture indicate that CYP suppresses Th2 and Th9 cell differentiation (Fig. 5). Collectively, these findings suggest that CYP inhibits OVA-induced DC maturation by targeting the PAK1-JNK-c-Jun/NF-κB signaling cascade, thereby downstream limiting the differentiation of Th2 and Th9 cells.

A suite of cytokines, including IL-4, IL-2 and IL-23, is essential for the differentiation of Th2 and/or Th9 subsets (47,48). Among these, IL-33 serves as a critical mediator in the pathogenesis of allergy and chronic inflammation (10). IL-33 signals through its cognate receptor ST2 (49), and the IL-33/ST2 axis has been fundamentally linked to Th2/Th9 differentiation and allergic airway inflammation (50-52). In the lung, IL-33 is highly expressed in macrophages, DCs and epithelial cells, with the highest levels observed in the former two populations. Conversely, no significant enhancement of IL-33 expression was observed in lung endothelial cells or fibroblast (Fig. S1). The current data demonstrate that CYP treatment reduces OVA-induced IL-33 secretion specifically in DCs (Fig. 5). Mechanistically, IL-33 promotes both Th2/Th9 differentiation (13,53) via the activation of NF-κB and JNK-c-Jun signaling pathways (13,47). While IL-33 facilitates T cell polarization toward Th2 and Th9 phenotypes, CYP effectively inhibits this IL-33-induced differentiation (Fig. 6). This is consistent with the present findings that IL-33 upregulates the phosphorylation of PAK1, NF-κB, JNK and c-Jun in Th2/Th9 cells, an effect that is reversed by CYP (Fig. 6). Furthermore, depletion IL-33 with an anti-IL-33 antibody attenuated OVA-induced lung inflammation. Notably, the OVA-induced influx Neu, macrophages, Eos, DCs and B cells were significantly diminished. Particularly, additional anti-IL-33 treatment led to a significant reduction in Th2/Th9 cell populations, while Th1/Th17 levels remained largely unaffected (Figs. S4 and 5). Collectively, these results suggest that CYP regulates T cell differentiation by inhibiting IL-33/ST2-induced PAK1 phosphorylation resulting in attenuating downstream JNK-c-Jun/NF-κB pathway. Beyond classical NF-κB signaling networks (51), it is reported for the first time, to the best of our knowledge, that CYP may directly bind to PAK1 in T cells. This binding prevents PAK1 phosphorylation, thereby inhibiting the T cell differentiation pathways associated with IL-33/ST2 signaling.

In summary, the present study demonstrates that CYP inhibits OVA-induced DCs maturation by suppressing the PAK1-JNK/NF-κB signaling pathway via the reduction of PAK1 phosphorylation. Furthermore, CYP targets PAK1 to attenuate Th2/Th9 differentiation by disrupting IL-33/ST2-PAK1-JNK/NF-κB networks (Fig. 7F). The primary contribution of this research is the identification of CYP as an effective modulator of the inflammatory response in allergic asthma, highlighting the critical role of PAK1 in regulating this underlying immunological mechanism. These findings offer a novel perspective on asthma prevention and management, positioning the PAK1 network as a viable therapeutic target and CYP as a promising new candidate for clinical intervention.

A limitation of the present study is that the investigation of CYP was restricted to the classical OVA-induced model of allergic asthma, a well-established paradigm extensively documented in literature (34,54). While the authors' laboratory actively utilizes house dust mite models in separate and ongoing CYP-related projects, evaluating these distinct experimental models fell outside the scope of the current manuscript. Future studies will be required to validate whether the CYP-mediated mechanisms observed here generalize across alternative models of asthma pathogenesis.

Acknowledgements

Not applicable.

Funding

The present study was supported by the Foundation of Luzhou Science and Technology Program and Southwest Medical University (grant no. 2024LZXNYDJ032), the Clinical Medicine Program of Southwest Medical University (grant nos. 2024LCYXZX50 and 2024LCYXZX25).

Availability of data and materials

The data generated in the present study may be requested from the corresponding author.

Authors' contributions

XW, KW and LLG conceived and designed the research. HH, XW, ZLZ, HMT, YZ and JD performed the experiments. HH and XW confirm the authenticity of all the raw data. XW, LLG, KW, HMT and HH analyzed the data. KW and LLG drafted the manuscript. LLG, KW and XW discussed, reviewed and edited the article. All authors read and approved the final version of the manuscript.

Ethics approval and consent to participate

All the *in vivo* related testing (including euthanasia) complied with the regulations and guidelines of the Southwest Medical University Institutional Animal Care Committee (approval nos. 20240417-002 and 20240701-007; Luzhou, China) and were performed according to the guidelines of AAALAC and IACUC.

Patient consent for publication

Not applicable.

Competing interests

The authors declare that they have no competing interests.

References

1. Morianos I and Semitekolou M: Dendritic cells: Critical regulators of allergic asthma. Int J Mol Sci 21: 7930, 2020.
2. Kuipers H and Lambrecht BN: The interplay of dendritic cells, Th2 cells and regulatory T cells in asthma. Curr Opin Immunol 16: 702-708, 2004.
3. Su XW, Lu G, Leung CK, Liu Q, Li Y, Tsang KS, Zhao SD, Chan DTM, Kung HF and Poon WS: miR-181d regulates human dendritic cell maturation through NF-κB pathway. Cell Prolif 50: e12358, 2017.
4. Huang B, He D, Chen G, Ran X, Guo W, Kan X, Wang W, Liu D, Fu S and Liu J: α-Cyperone inhibits LPS-induced inflammation in BV-2 cells through activation of Akt/Nrf2/HO-1 and suppression of the NF-κB pathway. Food Funct 9: 2735-2743, 2018.
5. Gao P, Ding N, Lv J, Ramzan MN and Wen Q: α-Cyperone inhibitory effects on tumor-derived DNA trigger microglia by STING pathway. J Ethnopharmacol 264: 113246, 2021.

6. Liu X, Jin X, Yu D and Liu G: Suppression of NLRP3 and NF-κB signaling pathways by α-Cyperone via activating SIRT1 contributes to attenuation of LPS-induced acute lung injury in mice. Int Immunopharmacol 76: 105886, 2019.
7. Kriehuber E, Bauer W, Charbonnier AS, Winter D, Amatschek S, Tamandl D, Schweifer N, Stingl G and Maurer D: Balance between NF-kappaB and JNK/AP-1 activity controls dendritic cell life and death. Blood 106: 175-183, 2005.
8. Liu W, Zi M, Naumann R, Ulm S, Jin J, Taglieri DM, Prehar S, Gui J, Tsui H, Xiao RP, *et al*: Pak1 as a novel therapeutic target for antihypertrophic treatment in the heart. Circulation 124: 2702-2715, 2011.
9. Sun H, Kamanova J, Lara-Tejero M and Galán JE: Salmonella stimulates pro-inflammatory signalling through p21-activated kinases bypassing innate immune receptors. Nat Microbiol 3: 1122-1130, 2018.
10. Cayrol C and Girard JP: Interleukin-33 (IL-33): A nuclear cytokine from the IL-1 family. Immunol Rev 281: 154-168, 2018.
11. Gabriele L, Schiavoni G, Mattei F, Sanchez M, Sestili P, Butteroni C, Businaro R, Mirchandani A, Niedbala W, Liew FY and Afferni C: Novel allergic asthma model demonstrates ST2-dependent dendritic cell targeting by cypress pollen. J Allergy Clin Immunol 132: 686-695.e7, 2013.
12. Chen J, Zhao Y, Jiang Y, Gao S, Wang Y, Wang D, Wang A, Yi H, Gu R, Yi Q and Wang S: Interleukin-33 contributes to the induction of Th9 cells and antitumor efficacy by dectin-1-activated dendritic cells. Front Immunol 9: 1787, 2018.
13. Alvarez F, Fritz JH and Piccirillo CA: Pleiotropic effects of IL-33 on $CD4^+$ T cell differentiation and effector functions. Front Immunol 10: 522, 2019.
14. Kurimoto M, Watanabe T, Kamata K, Minaga K and Kudo M: IL-33 as a critical cytokine for inflammation and fibrosis in inflammatory bowel diseases and pancreatitis. Front Physiol 12: 781012, 2021.
15. Riera-Martínez L, Cànaves-Gómez L, Iglesias A, Martin-Medina A and Cosío BG: The role of IL-33/ST2 in COPD and its future as an antibody therapy. Int J Mol Sci 24: 8702, 2023.
16. Chuang HC, Hsueh CH, Hsu PM, Tsai CY, Shih YC, Chiu HY, Chen YM, Yu WK, Chen MH and Tan TH: DUSP8 induces TGF-β-stimulated IL-9 transcription and Th9-mediated allergic inflammation by promoting nuclear export of Pur-α. J Clin Invest 133: e166269, 2023.
17. Wang X, Yang X, Li Y, Wang X, Zhang Y, Dai X, Niu B, Wu J, Yuan X, Xiong A, *et al*: Lyn kinase represses mucus hypersecretion by regulating IL-13-induced endoplasmic reticulum stress in asthma. EBioMedicine 15: 137-149, 2017.
18. Deng J, Tang H, Zhang Y, Yuan X, Ma N, Hu H, Wang X, Liu C, Xu G, Li Y, *et al*: House dust mite-induced endoplasmic reticulum stress mediates MUC5AC hypersecretion via TBK1 in airway epithelium. Exp Lung Res 49: 49-62, 2023.
19. Zhang Y, Guo L, Law BY, Liang X, Ma N, Xu G, Wang X, Yuan X, Tang H, Chen Q, *et al*: Resveratrol decreases cell apoptosis through inhibiting DNA damage in bronchial epithelial cells. Int J Mol Med 45: 1673-1684, 2020.
20. Tang H, Zhang Y, Wang Q, Zeng Z, Wang X, Li Y, Wang Z, Ma N, Xu G, Zhong X, *et al*: Astaxanthin attenuated cigarette smoke extract-induced apoptosis via decreasing oxidative DNA damage in airway epithelium. Biomed Pharmacother 167: 115471, 2023.
21. Guo L, Overholser J, Darby H, Ede NJ and Kaumaya PTP: A newly discovered PD-L1 B-cell epitope peptide vaccine (PDL1-Vaxx) exhibits potent immune responses and effective anti-tumor immunity in multiple syngeneic mice models and (synergizes) in combination with a dual HER-2 B-cell vaccine (B-Vaxx). Oncoimmunology 11: 2127691, 2022.
22. Wang Q, Guo L, Zeng Z, Huang Y, Tang H, Hu H, Yuan X, Deng J, Qin G, Wang X and Zhang Y: Neferine attenuates HDM-induced allergic inflammation by inhibiting the activation of dendritic cell. Inflammation 46: 2433-2448, 2023.
23. Livak KJ and Schmittgen TD: Analysis of relative gene expression data using real-time quantitative PCR and the 2(-Delta Delta C(T)) method. Methods 25: 402-408, 2001.
24. Benoit-Lizon I, Jacquin E, Rivera Vargas T, Richard C, Roussey A, Dal Zuffo L, Martin T, Melis A, Vinokurova D, Shahoei SH, *et al*: CD4 T cell-intrinsic STING signaling controls the differentiation and effector functions of T_H1 and T_H9 cells. J Immunother Cancer 10: e003459, 2022.
25. Tang Y, Wang X, Li Z, He Z, Yang X, Cheng X, Peng Y, Xue Q, Bai Y, Zhang R, *et al*: Heparin prevents caspase-11-dependent septic lethality independent of anticoagulant properties. Immunity 54: 454-467.e6, 2021.
26. Pelaia C, Vatrella A, Gallelli L, Lombardo N, Sciacqua A, Savino R and Pelaia G: Role of p38 mitogen-activated protein kinase in asthma and COPD: Pathogenic aspects and potential targeted therapies. Drug Des Devel Ther 15: 1275-1284, 2021.
27. Southworth T, Mason S, Bell A, Ramis I, Calbet M, Domenech A, Prats N, Miralpeix M and Singh D: PI3K, p38 and JAK/STAT signalling in bronchial tissue from patients with asthma following allergen challenge. Biomarker Res 6: 14, 2018.
28. Blom L, Poulsen BC, Jensen BM, Hansen A and Poulsen LK: IL-33 induces IL-9 production in human CD4+ T cells and basophils. PLoS One 6: e21695, 2011.
29. Reifs A, Fernandez-Calvo A, Alonso-Lerma B, Schönfelder J, Franco D, Ortega-Muñoz M, Casares S, Jimenez-Lopez C, Saa L, Cortajarena AL, *et al*: High-throughput virtual search of small molecules for controlling the mechanical stability of human CD4. J Biol Chem 300: 107133, 2024.
30. Fuchs C, Cosentino L, Urbinati C, Talamo MC, Medici G, Quattrini MC, Mottolese N, Pietraforte D, Fuso A, Ciani E and De Filippis B: Treatment with FRAX486 rescues neurobehavioral and metabolic alterations in a female mouse model of CDKL5 deficiency disorder. CNS Neurosci Ther 28: 1718-1732, 2022.
31. Tsai YR, Huang LJ, Lin HY, Hung YJ, Lee MR, Kuo SC, Hsu MF and Wang JP: Inhibition of formyl peptide-stimulated superoxide anion generation by Fal-002-2 occurs mainly through the blockade of the p21-activated kinase and protein kinase C signaling pathways in ratneutrophils. Eur J Pharmacol 701: 114-123, 2013.
32. Tjota MY, Hrusch CL, Blaine KM, Williams JW, Barrett NA and Sperling AI: Signaling through FcRγ-associated receptors on dendritic cells drives IL-33-dependent TH2-type responses. J Allergy Clin Immunol 134: 706-713.e8, 2014.
33. Koch S, Sopel N and Finotto S: Th9 and other IL-9-producing cells in allergic asthma. Semin Immunopathol 39: 55-68, 2017.
34. Guo H, Zhao Y, Zhang Z, Xu Y, Chen Y, Lei T and Zhao Y: The presence and pathogenic roles of M(IL-33 + IL-2) macrophages in allergic airway inflammation. Allergy 80: 1298-1308, 2025.
35. Rescigno M, Martino M, Sutherland CL, Gold MR and Ricciardi-Castagnoli P: Dendritic cell survival and maturation are regulated by different signaling pathways. J Exp Med 188: 2175-2180, 1998.
36. Handley ME, Thakker M, Pollara G, Chain BM and Katz DR: JNK activation limits dendritic cell maturation in response to reactive oxygen species by the induction of apoptosis. Free Radic Biol Med 38: 1637-1652, 2005.
37. Yu Q, Kovacs C, Yue FY and Ostrowski MA: The role of the p38 mitogen-activated protein kinase, extracellular signal-regulated kinase, and phosphoinositide-3-OH kinase signal transduction pathways in CD40 ligand-induced dendritic cell activation and expansion of virus-specific CD8+ T cell memory responses. J Immunol 172: 6047-6056, 2004.
38. Zheng T, Zhang B, Chen C, Ma J, Meng D, Huang J, Hu R, Liu X, Otsu K, Liu AC, *et al*: Protein kinase p38α signaling in dendritic cells regulates colon inflammation and tumorigenesis. Proc Natl Acad Sci USA 115: E12313-E12322, 2018.
39. Aksamitiene E, Achanta S, Kolch W, Kholodenko BN, Hoek JB and Kiyatkin A: Prolactin-stimulated activation of ERK1/2 mitogen-activated protein kinases is controlled by PI3-kinase/Rac/PAK signaling pathway in breast cancer cells. Cell Signal 23: 1794-1805, 2011.
40. Foryst-Ludwig A and Naumann M: p21-activated kinase 1 activates the nuclear factor kappa B (NF-kappa B)-inducing kinase-Ikappa B kinases NF-kappa B pathway and proinflammatory cytokines in Helicobacter pylori infection. J Biol Chem 275: 39779-39785, 2000.
41. Naumann M, Wessler S, Bartsch C, Wieland B, Covacci A, Haas R and Meyer TF: Activation of activator protein 1 and stress response kinases in epithelial cells colonized by Helicobacter pylori encoding the cag pathogenicity island. J Biol Chem 274: 31655-31662, 1999.
42. Chatterjee A, Ghosh J, Ramdas B, Mali RS, Martin H, Kobayashi M, Vemula S, Canela VH, Waskow ER, Visconte V, *et al*: Regulation of Stat5 by FAK and PAK1 in oncogenic FLT3- and KIT-driven leukemogenesis. Cell Rep 9: 1333-1348, 2014.
43. Wang J, Hirose H, Du G, Chong K, Kiyohara E, Witz IP and Hoon DSB: P-REX1 amplification promotes progression of cutaneous melanoma via the PAK1/P38/MMP-2 pathway. Cancer Lett 407: 66-75, 2017.

44. Yao D, Li C, Rajoka MSR, He Z, Huang J, Wang J and Zhang J: P21-Activated Kinase 1: Emerging biological functions and potential therapeutic targets in cancer. Theranostics 10: 9741-9766, 2020.
45. Dammann K, Khare V, Lang M, Claudel T, Harpain F, Granofszky N, Evstatiev R, Williams JM, Pritchard DM, Watson A and Gasche C: PAK1 modulates a PPARγ/NF-κB cascade in intestinal inflammation. Biochim Biophys Acta 1853: 2349-2360, 2015.
46. Orr AW, Hahn C, Blackman BR and Schwartz MA: p21-activated kinase signaling regulates oxidant-dependent NF-kappa B activation by flow. Circ Res 103: 671-679, 2008.
47. Kaplan MH: Th9 cells: Differentiation and disease. Immunol Rev 252: 104-115, 2013.
48. Harusato A, Abo H, Ngo VL, Yi SW, Mitsutake K, Osuka S, Kohlmeier JE, Li JD, Gewirtz AT, Nusrat A and Denning TL: IL-36γ signaling controls the induced regulatory T cell-Th9 cell balance via NFκB activation and STAT transcription factors. Mucosal Immunol 10: 1455-1467, 2017.
49. Schiering C, Krausgruber T, Chomka A, Fröhlich A, Adelmann K, Wohlfert EA, Pott J, Griseri T, Bollrath J, Hegazy AN, *et al*: The alarmin IL-33 promotes regulatory T-cell function in the intestine. Nature 513: 564-568, 2014.
50. Mangan NE, Dasvarma A, McKenzie AN and Fallon PG: T1/ST2 expression on Th2 cells negatively regulates allergic pulmonary inflammation. Eur J Immunol 37: 1302-1312, 2007.
51. Griesenauer B and Paczesny S: The ST2/IL-33 axis in immune cells during inflammatory diseases. Front Immunol 8: 475, 2017.
52. Hu J, Gao N, Zhang Y, Chen X, Li J, Bian F, Chi W, Liu Z, de Paiva CS, Pflugfelder SC and Li DQ: IL-33/ST2/IL-9/IL-9R signaling disrupts ocular surface barrier in allergic inflammation. Mucosal Immunol 13: 919-930, 2020.
53. Murakami-Satsutani N, Ito T, Nakanishi T, Inagaki N, Tanaka A, Vien PT, Kibata K, Inaba M and Nomura S: IL-33 promotes the induction and maintenance of Th2 immune responses by enhancing the function of OX40 ligand. Allergol Int 63: 443-455, 2014.
54. Song J, Zhang H, Tong Y, Wang Y, Xiang Q, Dai H, Weng C, Wang L, Fan J, Shuai Y, *et al*: Molecular mechanism of interleukin-17A regulating airway epithelial cell ferroptosis based on allergic asthma airway inflammation. Redox Biol 68: 102970, 2023.